# Surface Modification of $Li_{1.2}Ni_{0.13}Mn_{0.54}Co_{0.13}O_2$ by Hydrazine Vapor as Cathode Material for Lithium-Ion Batteries

Jie Zhang, Zhihong Lei, Jiulin Wang,* Yanna NuLi, and Jun Yang

Shanghai Electrochemical Energy Devices Research Center, Department of Chemical Engineering, Shanghai Jiao Tong University, 800 Dongchuan Road, Shanghai 200240, China

S *Supporting Information*
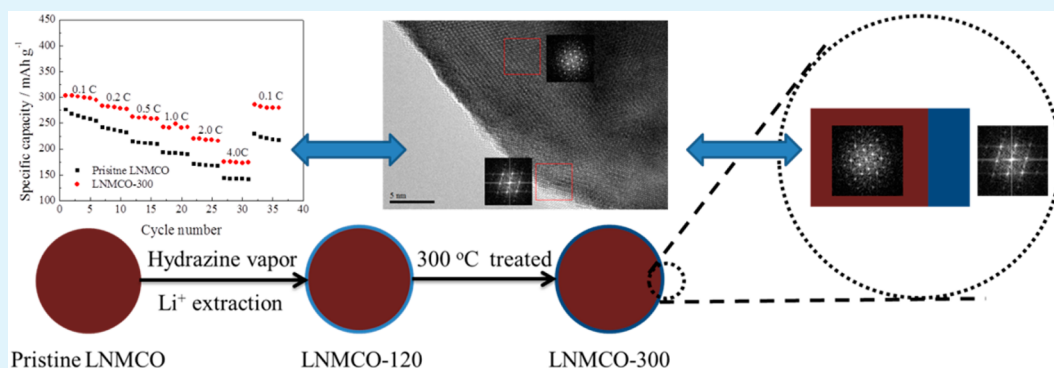
ABSTRACT: An artificial interface is successfully prepared on the surface of the layered lithium-rich cathode material $Li_{1.2}Ni_{0.13}Mn_{0.54}Co_{0.12}O_2$ via treating it with hydrazine vapor, followed by an annealing process. The inductively coupled plasma-atomic emission spectrometry (ICP) results indicate that lithium ions are leached out from the surface of $Li_{1.2}Ni_{0.13}Mn_{0.54}Co_{0.12}O_2$ by the hydrazine vapor. A lithium-deficiency-driven transformation from layered to spinel at the particle surface happens in the annealing process, which is proved by the results of X-ray diffraction (XRD) and high-resolution transmission electron microscope (HRTEM). It is also found that the content of the spinel phase increases at higher annealing temperature, and an internal structural evolution from $Li_{1-x}M_2O_4$-type spinel to M_3O_4-type spinel takes place simultaneously. Compared to the pristine $Li_{1.2}Ni_{0.13}Mn_{0.54}Co_{0.12}O_2$, the surface-modified sample annealed at 300 °C delivers a larger initial discharge capacity of 295.6 mA h g^{-1} with a Coulombic efficiency of 89.5% and a better rate performance (191.7 mA h g^{-1} at 400 mA g^{-1}).

KEYWORDS: *cathode material, lithium-rich material, surface modification, hydrazine vapor, lithium-ion battery*

1. INTRODUCTION

Present concerns about global warming and increased consumption of fossil energy have stimulated interest to develop electric vehicles (EVs), including hybrid electric vehicles (HEVs) and plug-in hybrid electric vehicles (PHEVs).[1,2] Lithium-ion batteries (LIBs) have been regarded as the most promising power sources for EVs. However, the currently commercialized LIBs cannot well satisfy the requirements of EVs with a long drive range due to their limited capacities of current cathode materials (<200 mA h g^{-1}), such as $LiCoO_2$, $LiFePO_4$, $LiNi_{1/3}Mn_{1/3}Co_{1/3}O_2$, and so on.[3-5] Therefore, it is urgent to develop cathode materials with low cost and high energy density for the next generation of LIBs.

In recent years, many cathode materials including layered lithium-rich materials, Ni-rich layered materials, and high-voltage spinel materials were investigated to substitute the traditional cathode materials.[6-8] Among these candidates, layered lithium-rich materials, represented by $xLi_2MnO_3 \cdot (1-x)LiMO_2$ (M = Mn, Co, Ni), have been considered as one of the promising candidates because of their high capacities (over

250 mA h g^{-1}). However, these materials suffer from some obvious drawbacks, such as large initial irreversible capacity, unstable cycling and poor rate performances, and the discharge voltage decay, which have to be overcome before their practical applications.[9-14]

Many efforts have been taken to enhance the electrochemical performance of lithium-rich materials. Surface coating is a common method to stabilize the cathode/electrolyte interface. Metal oxides (Al_2O_3,[15,16] MnO_x,[17] CeO_2[18]) and metal fluorite (AlF_3[19-21]) have been reported to effectively improve the electrochemical performance of lithium-rich materials, probably because of the stable surface coating layer. Li-contained oxides (Li_2SiO_3[22] and Li_2ZrO_3[23,24]), which have good conductivities and can provide Li^+ diffusion tunnel, have also enhanced the electrochemical performances of lithium-rich materials. Liu etc. reported a novel heterostructured $Li_{1.2}Ni_{0.13}Co_{0.13}Mn_{0.54}O_2$
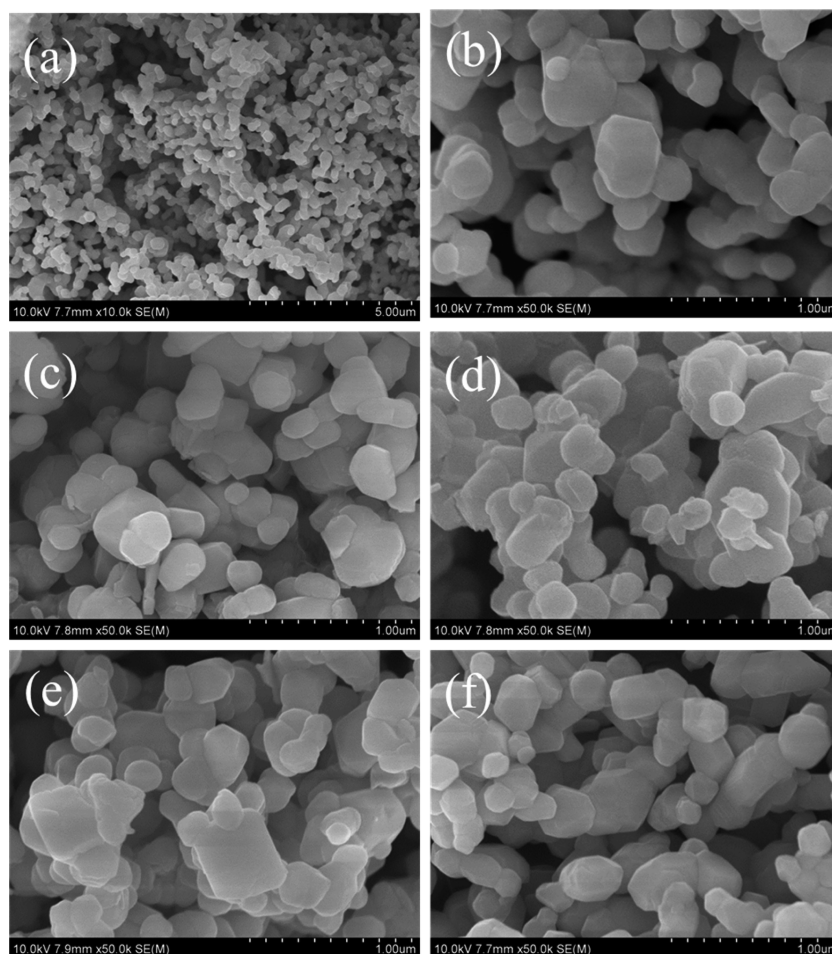
Figure 1. SEM images of (a, b) the pristine LNMCO, (c) LNMCO-120, (d) LNMCO-300, (e) LNMCO-500, and (f) LNMCO-700 samples.

material with mosaic spinel nanograins and surface coating by a one-step solid phase surface modification process, which exhibited an improved initial Coulombic efficiency and good cyclability.[25]

Another effective method to improve the electrochemical performance of lithium-rich materials is to synthesize the layered/spinel composites because of their structural compatibility with the same oxygen arrangement. The spinel structures, such as $LiMn_2O_4$[26] and $LiNi_{0.5}Mn_{1.5}O_4$,[27] have a three-dimensional diffusion path, which would theoretically have fast Li^+ diffusion through the active particle. Layered/spinel composites have been reported to take advantage of the merits of the layered and spinel materials while overcoming the drawbacks of each other.[28−30]

Generally, the atomic ratio of Li to transition metal in spinel materials ($LiMn_2O_4$ and $LiNi_{0.5}Mn_{1.5}O_4$) is less than 1. Similarly, the atomic ratio of O to transition metal ratio in spinel materials is also smaller than that of a typical lithium-rich material (e.g., $Li_{1.2}Mn_{0.54}Co_{0.13}Ni_{0.13}O_2$).[31] These phenomena indicate that a spinel component can be possibly formed through the removal of Li and O from the lithium-rich materials. Acid treatment is a common approach to remove Li and O from active materials. Thackeray et al. reported that Li_2O was chemically removed from the Li_2MnO_3 via an acid treatment of $0.3Li_2MnO_3·0.7LiMn_{0.333}Ni_{0.333}Co_{0.333}O_2$ with 0.1 M HNO_3.[32] Instead of acids, ammonium sulfate has also been reported to extract Li from the lithium-rich material through the decomposition of $(NH_4)_2SO_4$.[31] Recently, Cho et al.

treated lithium-rich material by a 0.4 wt % hydrazine solution, which chemically delithiated lithium ions from the Li_2MnO_3 phase, forming a spinel phase on the surface and resulting in a better electrochemical performance.[33,34] The concentration of hydrazine solution directly affects the treatment degree of the resulting material. Because of the low content of hydrazine (0.4 wt %), it may be difficult to obtain a uniform interface on the surface of the lithium-rich material.

Herein, a facile approach was proposed to transfer the layered surface into the spinel surface, resulting in a composite structure with a layer core and spinel surface. The lithium rich material $Li_{1.2}Ni_{0.13}Mn_{0.54}Co_{0.13}O_2$ was treated with hydrazine vapor, followed by a thermal treatment. The morphology and electrochemical performances of the modified materials were systematically investigated via XRD, ICP-OES, TEM, and half cells.

2. EXPERIMENTAL SECTION

2.1. Synthesis of $Li_{1.2}Ni_{0.13}Mn_{0.54}Co_{0.13}O_2$. Layered lithium-rich material $Li_{1.2}Ni_{0.13}Mn_{0.54}Co_{0.13}O_2$ was synthesized using spray drying, plus pyrolysis process.[35] $LiOH·H_2O$ (5 mol % excess), $Mn-(CH_3COO)_2·4H_2O$, $Co(CH_3COO)_2·4H_2O$, and $Ni(CH_3COO)_2·4H_2O$ with a molar ratio of 1.26:0.54:0.13:0.13 were dissolved in distilled water at room temperature, while citric acid as a chelating agent was added simultaneously. Then, the mixture solution was adjusted by ammonium hydroxide to pH 7. The final solution was dried via a spray dry instrument (B-290, Buchi). The dried precursor was annealed at 400 °C for 6 h, then grounded and calcined at 900 °C for 12 h in air to obtain the target $Li_{1.2}Mn_{0.54}Co_{0.13}Ni_{0.13}O_2$ material.
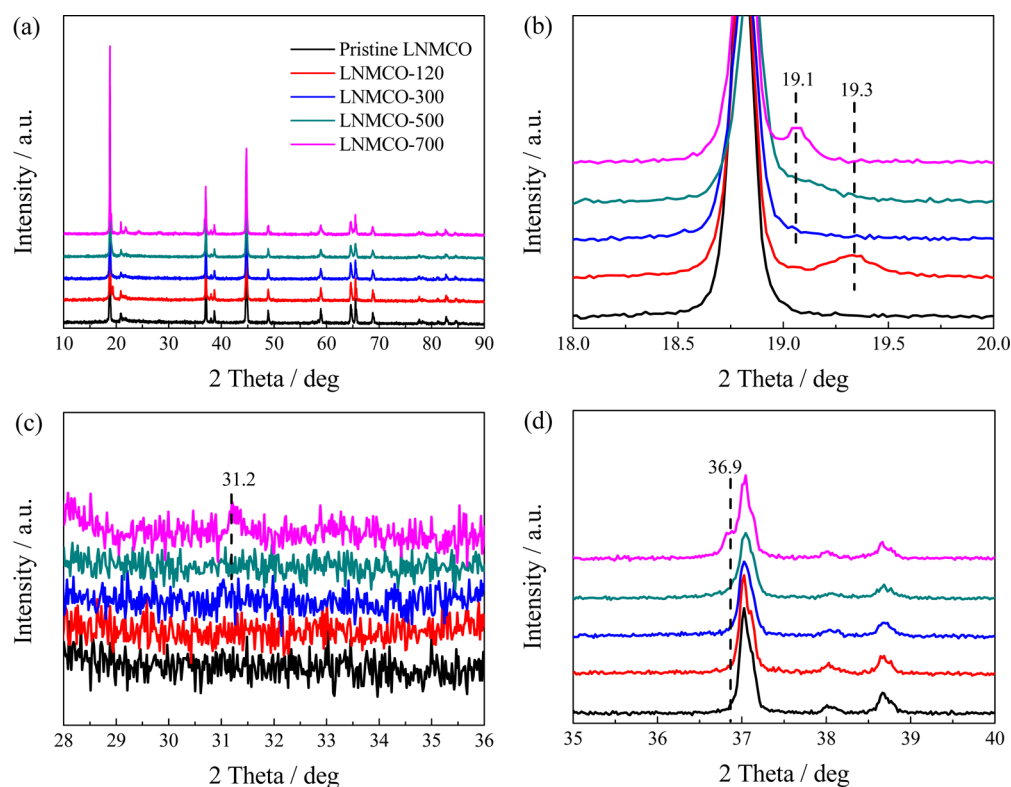
Figure 2. XRD patterns of the pristine LNMCO, LNMCO-120, LNMCO-300, LNMCO-500, and LNMCO-700 samples. (a) Entire range from 10 to 90° and (b−d) enlarged views.

Table 1. Chemical Compositions of the Pristine LNMCO and LNMCO-120 Samples

sample	Li	Ni	Mn	Co	calcd formula
LNMCO	8.204	7.509	29.14	7.688	$Li_{1.2}Ni_{0.13}Mn_{0.54}Co_{0.13}O_2$
LNMCO-120	7.728	7.522	29.37	7.851	$Li_{1.13}Ni_{0.13}Mn_{0.54}Co_{0.13}O_{2-x}$

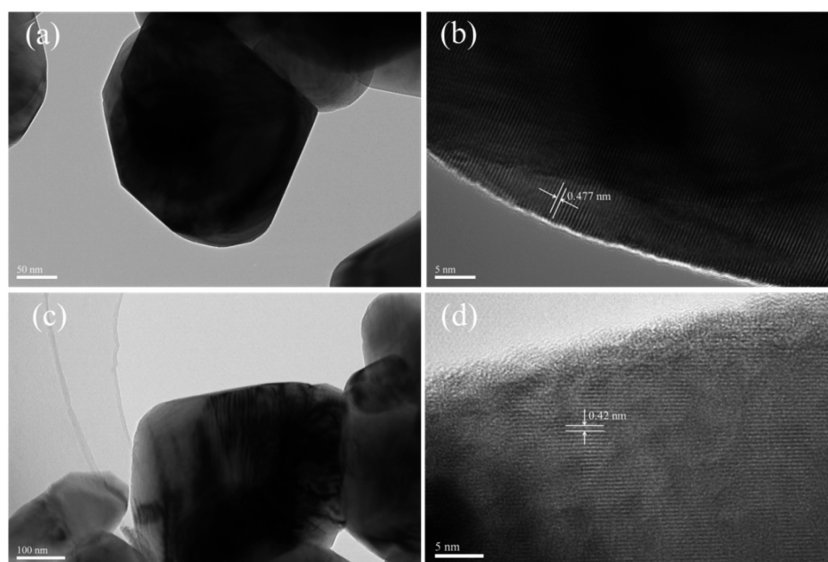**Figure 3.** TEM images of the pristine (a, b) LNMCO and (c, d) LNMCO-120 materials.

2.2. Surface-Treated $Li_{1.2}Ni_{0.13}Mn_{0.54}Co_{0.13}O_2$ by Hydrazine Vapor.

Three hundred milligrams of $Li_{1.2}Mn_{0.54}Co_{0.13}Ni_{0.13}O_2$ was put into a small glass vial, which was further placed in a glass bottle containing 10 mL of hydrazine monohydrate, without direct contact between the powder and the hydrazine monohydrate.[36] After sealing, the glass bottle was maintained at 120 °C for 2 h to let hydrazine vapor react with the $Li_{1.2}Mn_{0.54}Co_{0.13}Ni_{0.13}O_2$ material. After cooling, the product was washed with water for six times to remove the adsorbed hydrazine monohydrate and byproducts, followed by drying at 120 °C under vacuum overnight to obtain the hydrazine vapor treated $Li_{1.2}Mn_{0.54}Co_{0.13}Ni_{0.13}O_2$. Then, the treated material was annealed in a tube furnace at 300, 500, and 700 °C for 6 h. For convenience, the

pristine $Li_{1.2}Mn_{0.54}Co_{0.13}Ni_{0.13}O_2$, hydrazine vapor treated and subsequently thermally annealed materials are abbreviated as LNMCO and LNMCO-X (X means the treatment temperature), respectively.

2.3. Structural Characterizations. The crystal structure of sample was investigated by X-ray diffraction (XRD) using a D8 advance X-ray diffractometer with a Cu Kα radiation source (40 kV, 40 mA). The data were collected at a scan speed of 6 ° min^{-1} on the 2θ range from 10° to 90°. The morphology was observed by a field-emission scanning electron microscope (FE-SEM, S-4800, Hitachi). The field-emission transmission electron microscope (FE-TEM, JEM-2100F, JEOL) was used to detect the surface structural difference between LNMCO and LNMCO-X samples.

2.4. Electrochemical Characterizations. For the cathode fabrication, the active material was mixed with Super P and polyvinylidene fluoride (PVdF) binder in 1-methyl-2-pyrrolidinone (NMP) solvent with a weight ratio of 8:1:1. The electrochemical measurements of cathode were performed in lithium half cell (coin-type 2016) with a lithium foil as the anode, a PE separator, and 1 M LiPF$_6$ in ethylene carbonate (EC)/dimethyl carbonate (DMC) (1:1 by volume) as the electrolyte. All cells were assembled in an argon-filled glovebox with O$_2$ and H$_2$O contents less than 1 ppm. The galvanostatic charge/discharge and rate tests were conducted on a Land CT2001 battery test system in a voltage range of 2.0−4.8 V at 30 °C (1 C = 200 mA g^{-1}). Electrochemical impedance spectroscopy (EIS) was conducted on an electrochemical workstation (Autolab PGSTAT302N) in the frequency range from 0.01 Hz to 100 kHz with the amplitude of 10 mV.

3. RESULTS AND DISCUSSION

The SEM images of the pristine LNMCO and surface-modified samples are shown in Figure 1. For LMNCO powder, the polyhedral nanoparticle uniformly ranges between 200 and 400
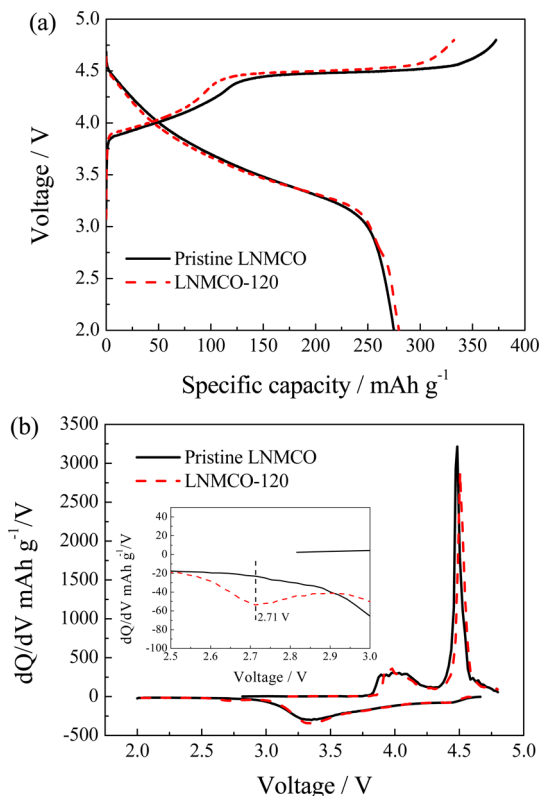

Figure 4. (a) Initial charge/discharge curves and (b) corresponding dQ/dV curves of the pristine LNMCO and LNMCO-120 samples cycled between 2.0 and 4.8 V at 20 mA g^{-1}.

nm (Figure 1a, b). The sharp edges and smooth planes indicate that the LNMCO material was highly crystallized. After surface treatment by hydrazine vapor and subsequently thermal annealing, there is no obvious morphology change in the surface-modified samples.

The powder XRD measurements were carried out to examine the structural changes between the pristine LNMCO and surface-modified samples. Figure 2a shows that all the reflections of the pristine LNCMO sample can be indexed to a typical layered structure with a rhombohedral $R\overline{3}m$ space group, except for the weak superlattice reflections located between 20° and 25°, which are well-known as a consequence of unique LiMn$_6$ ordering in the transition metal layer.[37] Slight differences can be found between the pristine and the modified samples. The LNMCO-120 sample shows a weak peak at around 19.3° (Figure 2b), which may be due to the intercalation of protons in the lithium layer.[38]

The Li, Mn, Co, and Ni contents of the pristine LNMCO and LNMCO-120 samples were determined by ICP (normalized to the Mn content), as shown in Table 1. The chemical formula of the pristine LNMCO sample is identical to the ideal $Li_{1.2}Ni_{0.13}Mn_{0.54}Co_{0.13}O_2$ chemical stoichiometry. The ICP results of the LNCMO-120 in Table 1 confirm that lithium ions have been successfully extracted by hydrazine vapor at 120 °C.

After a thermal treatment at 300 °C, the 19.3° peak in the LNMCO-120 disappeared, indicating that the incorporated protons are unstable and will evolve at elevated temperature. The removal of incorporated protons from the surface lattice leads to the formation of lithium vacancies. When annealed at high temperatures (500 and 700 °C), new peaks at 19.1 (Figure 2b) and 36.8° (Figure 2c) appeared, which are similar to the diffractions from (111) and (311) in Li$_{1-x}$Mn$_2$O$_4$ spinel structure. A small peak at 31.2° (Figure 2d) in the LNMCO-700 sample indicates that the Li$_{1-x}$Mn$_2$O$_4$ spinel might undergo an inner phase transition to form the M$_3$O$_4$-type spinel phase at high annealing temperature, which is attributed to the migration of transition metal ions from the 16d octahedral sites to the 8a tetrahedral sites in $Fd\overline{3}m$ symmetry.[39,40]

There are two phases (LiNi$_{1/3}$Mn$_{1/3}$Co$_{1/3}$O$_2$ and Li$_2$MnO$_3$) in the pristine LNMCO material. In order to distinguish which phase reacts with hydrazine vapor, commercialized Li-Ni$_{1/3}$Mn$_{1/3}$Co$_{1/3}$O$_2$, which is one of the phases in the LNMCO material, was also treated by hydrazine vapor at 120 °C. Its XRD pattern (Figure S1 in the Supporting Information) demonstrates that no peak appears at 19.3 °, indicating almost no Li$^+$/H$^+$ ion-exchange between LiNi$_{1/3}$Mn$_{1/3}$Co$_{1/3}$O$_2$ and hydrazine vapor. Therefore, it is reasonable to speculate that the other Li$_2$MnO$_3$ phase was chemically delithiated by the hydrazine vapor.

Figure 3 displays the TEM images of the pristine LNMCO and LNMCO-120 samples to further detect the structural change by hydrazine vapor treatment. Both the surfaces of the pristine LNMCO and LNMCO-120 samples are smooth (Figure 3a, c), indicating the moderate reaction between LNMCO and hydrazine vapor without severe surface destruction. Typical layered fringes of the pristine LNMCO presented in the HRTEM image (Figure 3b) are straight and continuous to the particle surface. By contrast, the surface structure of the LNMCO-120 is different from that of the pristine LNMCO. As shown in Figure 3d, a coating layer in ca. 3 nm thickness successfully formed on the surface of the
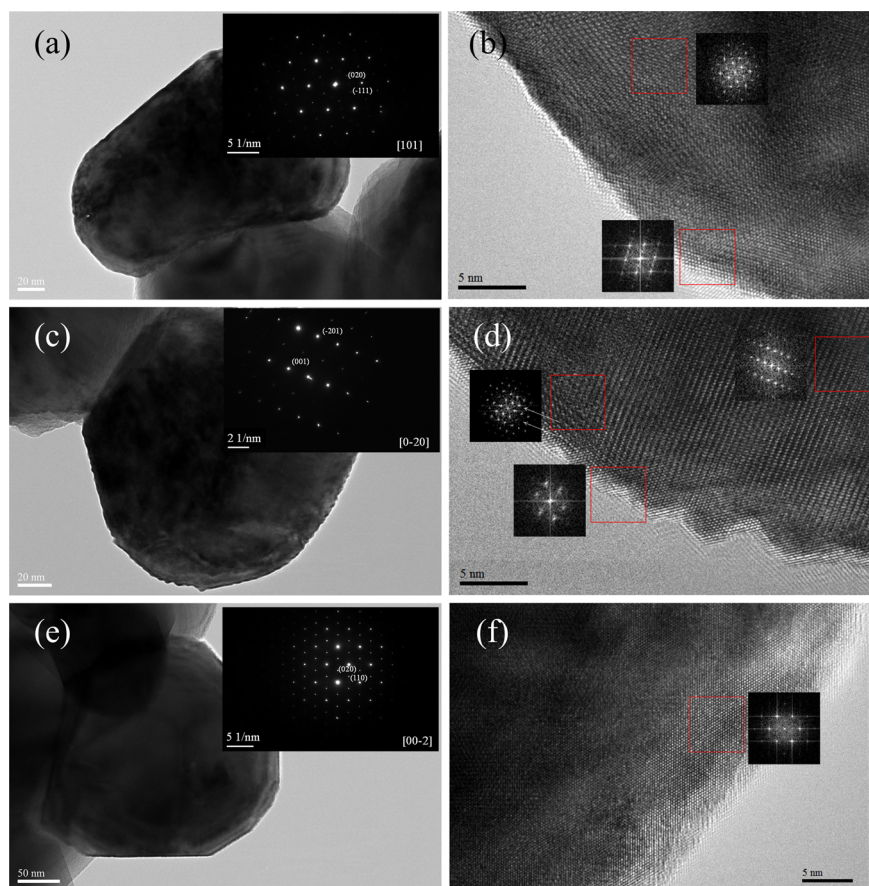
Figure 5. TEM and SAED images of the (a, b) LNMCO-300, (c, d) LNMCO-500, and (e, f) LNMCO-700 materials.

LNMCO-120 via the reaction between hydrazine vapor and the LNMCO material.

The initial charge/discharge curves of the pristine LNMCO and LNMCO-120 samples between 2.0 and 4.8 V at 20 mA g^{-1} and their corresponding dQ/dV plots are shown in Figure 4. The pristine sample demonstrates a typical profile of layered lithium-rich materials, including a sloping curve below 4.5 V and a plateau around 4.5 V in charge process and a continuous sloping curve in discharge process. The pristine LNMCO shows a discharge capacity of 268.5 mA h g^{-1} with only 73.4% columbic efficiency, which mainly derives from the irreversible Li$^+$ extraction (Li$_2$O) from the Li$_2$MnO$_3$ phase on the 4.5 V plateau during the initial charge process. Previous reports elucidate that surface structure damage by Li$^+$/H$^+$ exchange is unavoidable, leading to deteriorated electrochemical performances.[40,41] Interestingly, compared to its precursor, the LNMCO-120 sample displays similar charge/discharge profiles and larger discharge capacity. The initial discharge specific capacity and Coulombic efficiency of the LNMCO-120 are 279.7 mA h g^{-1} and 84.2%, respectively. All of them are improved after the hydrazine vapor treatment.

Figure 4b shows the dQ/dV plots of the initial charge/discharge profile of the pristine LNMCO and LNMCO-120 samples. In the initial oxidation process of the pristine LNMCO, the anodic peak at ~4.0 V can be ascribed to the extraction of lithium ions from the layered Li-Ni$_{1/3}$Co$_{1/3}$Mn$_{1/3}$O$_2$ phase accompanied by the oxidation of Ni^{2+} and Co^{3+} ions, and a sharp peak at 4.48 V corresponds to the loss of Li$_2$O from the Li$_2$MnO$_3$ phase to form an electrochemical active layered MnO$_2$ phase. In the following

cathodic process, the voltage range from 4.5 to 3.5 V corresponds to the reduction of Ni^{4+} and Co^{4+}, whereas the reduction peak at ~3.30 V is assigned to the reduction of MnO$_2$ (Mn^{4+}).[37] The activated peak of the Li$_2$MnO$_3$ phase in the LNMCO-120 shows a slight shift (0.02 V) to high voltage due to the existence of protons in the surface structure, which block the migration of Li$^+$ from the bulk to electrolyte.[41] Besides, a cathodic peak corresponding to the newly formed surface phase by hydrazine vapor treatment appears at 2.71 V, indicating the slight reconstruction of surface structure through the migration of transition metal ions to lithium layer. Based on the above analysis, the factors which enhanced initial Coulombic efficiency and capacity of LNMO-120 material can be listed as (1) part of lithium ions were extracted from Li$_2$MnO$_3$ by hydrazine vapor, so the irreversible charge capacity decrease with a short 4.5 V plateau, resulting in a higher Coulombic efficiency; (2) the electrochemical active surface layer provides extra Li$^+$ intercalating sites at 2.71 V, leading to a higher discharge capacity.

To remove the incorporated protons, we annealed the LNMCO-120 sample at 300, 500, and 700 °C for 6h in air, respectively. The TEM and SAED images of LNMCO-300, LNMCO-500, and LNMCO-700 highlight the effects of heat treatment on the LNMCO-120 material in Figure 5. Local structure information extracted from the HRTEM image marked by red box using a Fast Fourier Transform (FFT) is shown in Figure 5b, d, and f. As shown in Figure 5b, the lattice arrangement at the interface of the LNMCO-300 sample is extremely different to that at the inner particle. The FFT pattern of surface region in LNMCO-300 (Figure 5b) matches
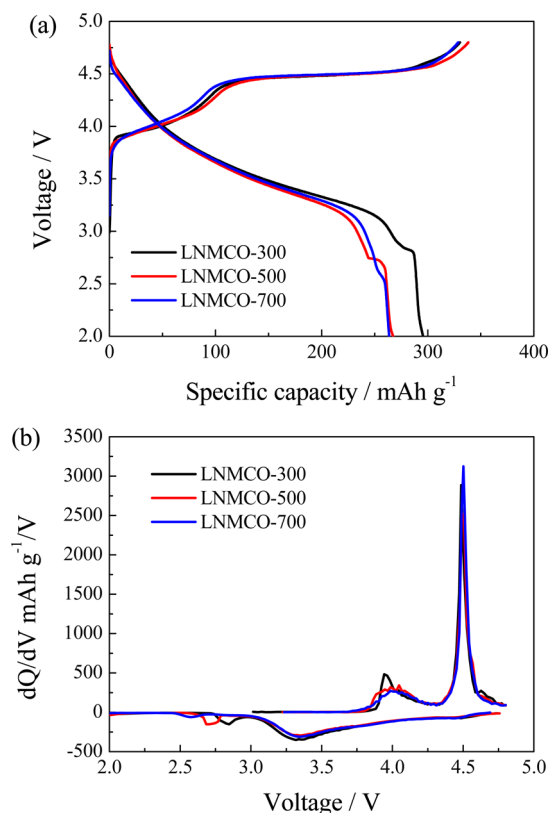
Figure 6. (a) Initial charge/discharge and (b) corresponding dQ/dV curves of the LNMCO-300, LNMCO-500, and LNMCO-700 samples cycled between 2.0 and 4.8 V at 20 mA g^{-1}.

Figure 7. (a) Cycling performance of the pristine LNMCO, LNMCO-120, LNMCO-300, LNMCO-500, and LNMCO-700 samples between 2.0 and 4.8 V at the current rate of 0.1 C (1 C = 200 mA g^{-1}); (b) rate capability of the pristine LNMCO, LNMCO-120, LNMCO-300, LNMCO-500, and LNMCO-700 samples at various discharging current rates after charging at 0.1 C rate to 4.8 V.

that of a spinel-like phase along the spinel [110] direction (Figure S2a in the Supporting Information).[34] In Figure 5d, the HRTEM and FFT images reveal several different domains in the LNMCO-500. The FFT pattern from inner region show only the reflections from layered structure, whereas the FFT patterns from the surface regions exhibit additional reflections that can be indexed to a spinel component (Figure S2b in the Supporting Information).[42] The row of spots indicated by the white arrow in Figure 5d also corresponds to a spinel configuration.[30] As for the LNMCO-700 sample, the surface spinel region is greatly enlarged, probably because of the reaction between the bulk and surface layer. At 700 °C, more transition metal ions migrate from the transition metal layer into the lithium layer to form the spinel phase, which is consistent with the XRD results.

The initial charge/discharge curves and corresponding dQ/dV plots of the LNMCO-300, LNMCO-500, and LNMCO-700 samples are shown in Figure 6. Compared to the LNMCO-120, the LNMCO-300 sample exhibits higher initial discharge specific capacity (295.6 mAh g^{-1}) and Coulombic efficiency (89.5%) with an obvious 2.8 V voltage platform, which is a characteristic plateau of spinel-like phase corresponding to the insertion of Li$^+$ into the empty 16c octahedral sites. At 300 °C, the incorporated protons are removed and lithium vacancies are formed in surface lattice, which induce migration of more transition metal ions from the transition metal layer to the lithium layer and formation of more spinel component. This spinel-like feature is clearly evident in the corresponding dQ/dV plot in Figure 4b, in which a sharp reduction peak centered at ~2.8 V is observed.
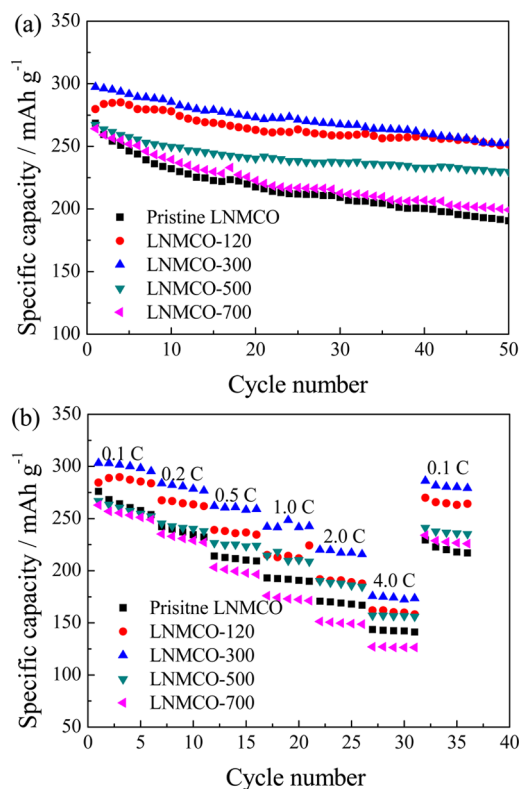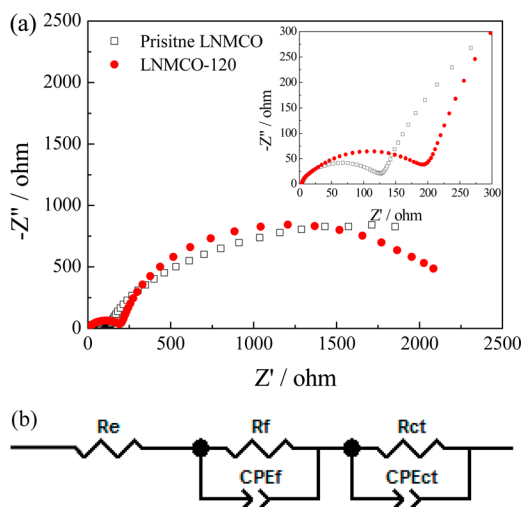

Figure 8. (a) Nyquist plots of the pristine LNMCO and LNMCO-120 electrodes after initial charged to 4.8 V at 0.1 C; (b) equivalent circuit used for analysis of experimental data.

Further increasing the annealed temperature to 500 and 700 °C, the spinel voltage platform undergoes a descending process from 2.8 to 2.6 V. The slight difference in the discharge plateau may be ascribed to the structural evolution from Li$_{1-x}$M$_2$O$_4$-type spinel structure to M$_3$O$_4$-type spinel structure upon calcination. Unlike the Li$_{1-x}$M$_2$O$_4$-type spinel structure with three-dimensional lithium ion diffusion channel, the M$_3$O$_4$-type
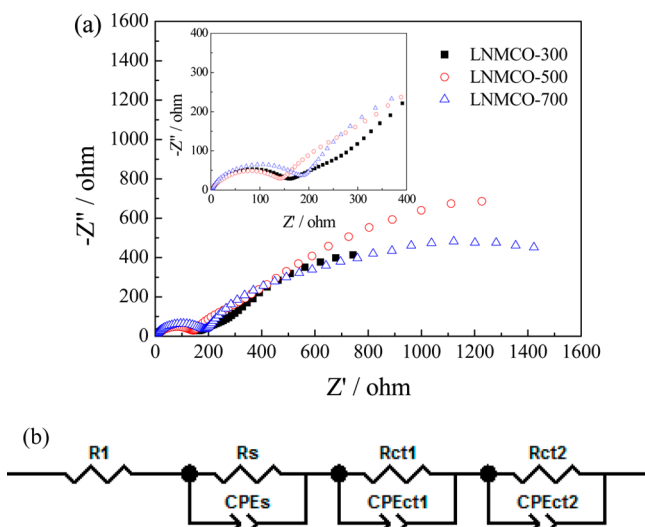
Figure 9. (a) Nyquist plots of the LNMCO-300, LNMCO-500 and LNMCO-700 electrodes after initial charged to 4.8 V at 0.1 C; (b) equivalent circuit used for analysis of experimental data.

spinel structure with both tetrahedral- and octahedral-sites occupied by the transition metal atoms, shows very low lithium ion conductivity. Therefore, the initial discharge capacity decreases gradually with the enhanced annealing temperature rising from 300 (295.6 mA h g^{-1}) to 700 °C (263.7 mA h g^{-1}). The corresponding initial Coulombic efficiency also decreases from 89.5% (300 °C) to 80.2% (700 °C). The spinel plateau below 3.0 V is still obvious in the second cycle (Figure S3 in the Supporting Information), indicating that the surface spinel phase can reversibly insert/extract lithium ions.

The cycling stability and rate performances of the pristine LNMCO and the surface modified LNMCO samples between 2.0 and 4.8 V are shown in Figure 7. The pristine LNMCO exhibits a gradual capacity fade upon cycling and the discharge capacity decreases from 265.8 mA h g^{-1} in the first cycle to 190.5 mA h g^{-1} after 50 cycles in Figure. 7a. The unstable electrode/electrolyte interface may be responsible for this fading. First, the carbonate-based electrolyte is unstable and can be decomposed at high voltage (>4.5 V). Second, the +4 transition metals (Ni or Co) in the charged material can react with electrolyte, leading the solution of transition metal and decomposition of electrolyte.[35] Compared with the pristine LNMCO, the LNMCO-120 and LNMCO-300 samples deliver larger discharge capacities in the initial cycle, but exhibit similar capacity retention. Despite the formation of spinel phase on the particle surface, such a surface is still sensitive to electrolyte at high voltage. Therefore, the cyclic stability of surface modified materials has not been apparently improved because no protection layers have been formed through such modification. All samples show obvious voltage decay during cycling (Figure S4a in the Supporting Information), indicating that the slight surface spinel phase cannot fundamentally suppress the structure transformation. The LNMCO-300 sample shows the highest specific energy density of 816.5 W h kg^{-1} after 50 cycles (Figure S4b in the Supporting Information).

Figure 7b compares the rate capability of the pristine and the surface treated LNMCO samples. The data are collected by charging at 0.1 C and discharging at various rates (0.1, 0.2, 0.5, 1.0, 2.0, and 4.0 C). The LNMCO-300 sample manifests best rate performance. Especially at 2.0 C charge/discharge rate,

it can exhibit a maximal capacity of 191.7 mA h g^{-1}, much higher than that of the pristine sample (170.7 mA h g^{-1}).

To understand the improvement in rate capability, we carried out electrochemical impedance spectra (EIS) measurement on the pristine LNMCO and the surface-treated LNMCO electrodes. Before the EIS measurement, the fresh electrodes were initially charged to 4.8 V at a current of 20 mA g^{-1} to reach an identical status. The EIS plots of LNMCO and LNMCO-120 materials (Figure 8a) display a semicircle at high frequency and an arc in the low frequency. In the equivalent circuit (Figure 8b), R_e is the ohmic resistance, R_s and CPE$_s$ represent the lithium ion diffusion resistance and capacitance in solid electrolyte interphase (SEI), R_{ct} and CPE$_{ct}$ correspond to the charge-transfer resistance and double-layer capacitance in the electrode/SEI layer.[35] Because of the newly formed proton-incorporated surface layer on the surface of LNMCO-120, the surface layer resistance increased significantly from 121.0 Ω in the pristine LNMCO electrode to 199.2 Ω in the LNMCO-120 electrode.

The EIS plots of LNMCO-300, LNMCO-500 and LNMCO-700 materials (Figure 9a) display two arcs in the low frequency, which may be ascribed to the formation of surface spinel phase. There are spinel/SEI layer and layered/spinel interfaces on the surface, leading to two kinds of charge-transfer resistance. In the equivalent circuit (Figure 9b), R_{ct1} and R_{ct2} correspond to the charge-transfer resistance in the spinel phase and layered phase, respectively. The fitting results of LNMCO-300, LNMCO-500 and LNMCO-700 materials are shown in the Supporting Information, Figure S5. The charge-transfer resistance in spinel phase and layered phase on surface of the LNMCO-300 electrode are 245 and 1250 Ω respectively, suggesting that the spinel coating can lower the surface charge transfer resistance and accelerate the lithium-ion diffusion. When further raise the annealed temperature to 500 °C, the charge transfer resistances (R_{ct1} and R_{ct2}) significantly increase to 300 and 2300 Ω, probably because of the formation of M$_3$O$_4$ phase.

4. CONCLUSION

In this work, hydrazine vapor was employed to extract lithium ions from the surface region of the layered lithium rich material Li$_{1.2}$Ni$_{0.13}$Mn$_{0.54}$Co$_{0.13}$O$_2$ (LNMCO). The active Li$_2$MnO$_3$ in the LNMCO phase reacted with hydrazine vapor. A Li-deficient and proton-incorporated layer was formed on the surface of LNMCO-120. The removal of the incorporated protons and migration of transition metal ions from the transition metal layer into the lithium layer at 300 °C resulted in a spinel Li$_{1-x}$M$_2$O$_4$ phase on the surface of LNMCO-300. Higher thermal treatment temperature induced an internal structure evolution from the spinel Li$_{1-x}$M$_2$O$_4$ phase to the M$_3$O$_4$-type spinel phase. Benefited by the artificial spinel layer generated by hydrazine vapor and 300 °C annealing treatments, the initial Coulombic efficiency, discharge capacity, and rate capability of the lithium-rich material have been significantly improved.

■ ASSOCIATED CONTENT

Ⓢ Supporting Information

The XRD patterns of the pristine and hydrazine vapor-treated LiNi$_{1/3}$Mn$_{1/3}$Co$_{1/3}$O$_2$ sample at 120 °C. Simulated SAED patterns of Fd$\overline{3}$m spinel phase along [110] and [−411] zone axis. The second charge/discharge profiles of the pristine LNMCO, LNMCO-120, LNMCO-300, LNMCO-500, and LNMCO-700 samples cycled between 2.0 and 4.8 V at 20

mA g^{-1}. The average discharge voltage and energy density of the pristine LNMCO, LNMCO-120, LNMCO-300, LNMCO-500, and LNMCO-700 samples cycled between 2.0 and 4.8 V at 20 mA g^{-1}. The EIS plots and fitting results of the LNMCO-300, LNMCO-500, and LNMCO-700 electrodes after initial charged to 4.8 V at 0.1 C. The Supporting Information is available free of charge on the ACS Publications website at DOI: 10.1021/acsami.5b02937.

■ AUTHOR INFORMATION

Corresponding Author

* E-mail: wangjiulin@sjtu.edu.cn. Tel: (+86)21-54745887. Fax: (+86)21-54747667.

Notes

The authors declare no competing financial interest.

■ REFERENCES

(1) Chu, S.; Majumdar, A. Opportunities and Challenges for a Sustainable Energy Future. *Nature* **2012**, *488*, 294−303.

(2) Goodenough, J. B. Electrochemical Energy Storage in a Sustainable Modern Society. *Energy Environ. Sci.* **2014**, *7*, 14−18.

(3) Dai, X.; Wang, L.; Xu, J.; Wang, Y.; Zhou, A.; Li, J. Improved Electrochemical Performance of LiCoO$_2$ Electrodes with ZnO Coating by Radio Frequency Magnetron Sputtering. *ACS Appl. Mater. Interfaces* **2014**, *6*, 15853−15859.

(4) Yuan, L.-X.; Wang, Z.-H.; Zhang, W.-X.; Hu, X.-L.; Chen, J.-T.; Huang, Y.-H.; Goodenough, J. B. Development and Challenges of LiFePO$_4$ Cathode Material for Lithium-Ion Batteries. *Energy Environ. Sci.* **2011**, *4*, 269−284.

(5) Jiang, K.-C.; Xin, S.; Lee, J.-S.; Kim, J.; Xiao, X.-L.; Guo, Y.-G. Improved Kinetics of LiNi$_{1/3}$Mn$_{1/3}$Co$_{1/3}$O$_2$ Cathode Material through Reduced Graphene Oxide Networks. *Phys. Chem. Chem. Phys.* **2012**, *14*, 2934−2939.

(6) Yabuuchi, N.; Yoshii, K.; Myung, S.-T.; Nakai, I.; Komaba, S. Detailed Studies of a High-Capacity Electrode Material for Rechargeable Batteries, Li$_2$MnO$_3$-LiCo$_{1/3}$Ni$_{1/3}$Mn$_{1/3}$O$_2$. *J. Am. Chem. Soc.* **2011**, *133*, 4404−4419.

(7) Lee, S.-H.; Yoon, C. S.; Amine, K.; Sun, Y.-K. Improvement of Long-Term Cycling Performance of Li[Ni$_{0.8}$Co$_{0.15}$Al$_{0.05}$]O$_2$ by AlF$_3$ Coating. *J. Power Sources* **2013**, *234*, 201−207.

(8) Fang, X.; Shen, C.; Ge, M.; Rong, J.; Liu, Y.; Zhang, A.; Wei, F.; Zhou, C. High-Power Lithium Ion Batteries Based on Flexible and Light-Weight Cathode of LiNi$_{0.5}$Mn$_{1.5}$O$_4$/Carbon Nanotube Film. *Nano Energy* **2015**, *12*, 43−51.

(9) Hy, S.; Felix, F.; Rick, J.; Su, W.-N.; Hwang, B. J. Direct*In situ*Observation of Li$_2$O Evolution on Li-Rich High-Capacity Cathode Material, Li[Ni$_x$Li$_{(1−2x)/3}$Mn$_{(2-x)/3}$]O$_2$ (0 ≤ x ≤ 0.5). *J. Am. Chem. Soc.* **2014**, *136*, 999−1007.

(10) Martha, S. K.; Nanda, J.; Veith, G. M.; Dudney, N. J. Electrochemical and Rate Performance Study of High-Voltage Lithium-Rich Composition: Li$_{1.2}$Mn$_{0.525}$Ni$_{0.175}$Co$_{0.1}$O$_2$. *J. Power Sources* **2012**, *199*, 220−226.

(11) Zheng, J.; Shi, W.; Gu, M.; Xiao, J.; Zuo, P.; Wang, C.; Zhang, J. G. Electrochemical Kinetics and Performance of Layered Composite Cathode Material Li[Li$_{0.2}$Ni$_{0.2}$Mn$_{0.6}$]O$_2$. *J. Electrochem. Soc.* **2013**, *160*, A2212−A2219.

(12) Sathiya, M.; Abakumov, A. M.; Foix, D.; Rousse, G.; Ramesha, K.; Saubanère, M.; Doublet, M. L.; Vezin, H.; Laisa, C. P.; Prakash, A.

S.; Gonbeau, D.; VanTendeloo, G.; Tarascon, J. M. Origin of Voltage Decay in High-Capacity Layered Oxide Electrodes. *Nat. Mater.* **2015**, *14*, 230−238.

(13) Choi, N.-S.; Han, J.-G.; Ha, S.-Y.; Park, I.; Back, C.-K. Recent Advances in the Electrolytes for Interfacial Stability of High-Voltage Cathodes in Lithium-Ion Batteries. *RSC Adv.* **2015**, *5*, 2732−2748.

(14) Yu, H.; Kim, H.; Wang, Y.; He, P.; Asakura, D.; Nakamura, Y.; Zhou, H. High-Energy 'Composite' Layered Manganese-Rich Cathode Materials via Controlling Li$_2$MnO$_3$ Phase Activation for Lithium-Ion Batteries. *Phys. Chem. Chem. Phys.* **2012**, *14*, 6584−6595.

(15) Zhang, X.; Belharouak, I.; Li, L.; Lei, Y.; Elam, J. W.; Nie, A.; Chen, X.; Yassar, R. S.; Axelbaum, R. L. Structural and Electrochemical Study of Al$_2$O$_3$ and TiO$_2$ Coated Li$_{1.2}$Ni$_{0.13}$Mn$_{0.54}$Co$_{0.13}$O$_2$ Cathode Material Using ALD. *Adv. Energy Mater.* **2013**, *3*, 1299−1307.

(16) He, W.; Qian, J.; Cao, Y.; Ai, X.; Yang, H. Improved Electrochemical Performances of Nanocrystalline Li-[Li$_{0.2}$Mn$_{0.54}$Ni$_{0.13}$Co$_{0.13}$]O$_2$ Cathode Material for Li-Ion Batteries. *RSC Adv.* **2012**, *2*, 3423−3429.

(17) Wu, F.; Li, N.; Su, Y.; Lu, H.; Zhang, L.; An, R.; Wang, Z.; Bao, L.; Chen, S. Can Surface Modification Be More Effective to Enhance the Electrochemical Performance of Lithium Rich Materials? *J. Mater. Chem.* **2012**, *22*, 1489−1497.

(18) Yuan, W.; Zhang, H. Z.; Liu, Q.; Li, G. R.; Gao, X. P. Surface Modification of Li(Li$_{0.17}$Ni$_{0.2}$Co$_{0.05}$Mn$_{0.58}$)O$_2$ with CeO$_2$ as Cathode Material for Li-Ion Batteries. *Electrochim. Acta* **2014**, *135*, 199−207.

(19) Sun, Y.-K.; Lee, M.-J.; Yoon, C. S.; Hassoun, J.; Amine, K.; Scrosati, B. The Role of AlF$_3$ Coatings in Improving Electrochemical Cycling of Li-Enriched Nickel-Manganese Oxide Electrodes for Li-Ion Batteries. *Adv. Mater.* **2012**, *24*, 1192−1196.

(20) Zhao, T.; Chen, S.; Chen, R.; Li, L.; Zhang, X.; Xie, M.; Wu, F. The Positive Roles of Integrated Layered-Spinel Structures Combined with Nanocoating in Low-Cost Li-Rich Cathode Li-[Li$_{0.2}$Fe$_{0.1}$Ni$_{0.15}$Mn$_{0.55}$]O$_2$ for Lithium-Ion Batteries. *ACS Appl. Mater. Interfaces* **2014**, *6*, 21711−21720.

(21) Zheng, J.; Gu, M.; Xiao, J.; Polzin, B. J.; Yan, P.; Chen, X.; Wang, C.; Zhang, J.-G. Functioning Mechanism of AlF$_3$ Coating on the Li- and Mn-Rich Cathode Materials. *Chem. Mater.* **2014**, *26*, 6320−6327.

(22) Zhao, E.; Liu, X.; Zhao, H.; Xiao, X.; Hu, Z. Ion Conducting Li$_2$SiO$_3$-Coated Lithium-Rich Layered Oxide Exhibiting High Rate Capability and Low Polarization. *Chem. Commun.* **2015**, *51*, 9093−9096.

(23) Zhang, X.; Sun, S.; Wu, Q.; Wan, N.; Pan, D.; Bai, Y. Improved Electrochemical and Thermal Performances of Layered Li-[Li$_{0.2}$Ni$_{0.17}$Co$_{0.07}$Mn$_{0.56}$]O$_2$ via Li$_2$ZrO$_3$ Surface Modification. *J. Power Sources* **2015**, *282*, 378−384.

(24) Miao, X.; Ni, H.; Zhang, H.; Wang, C.; Fang, J.; Yang, G. Li$_2$ZrO$_3$-Coated 0.4Li$_2$MnO$_3$·0.6LiNi$_{1/3}$Co$_{1/3}$Mn$_{1/3}$O$_2$ for High Performance Cathode Material in Lithium-Ion Battery. *J. Power Sources* **2014**, *264*, 147−154.

(25) Liu, H.; Du, C.; Yin, G.; Song, B.; Zuo, P.; Cheng, X.; Ma, Y.; Gao, Y. A Li-Rich Oxide Cathode Material with Mosaic Spinel Grain and Surface Coating for High Performance Li-Ion Batteries. *J. Mater. Chem. A* **2014**, *2*, 15640−15646.

(26) Tang, D.; Sun, Y.; Yang, Z.; Ben, L.; Gu, L.; Huang, X. Surface Structure Evolution of LiMn$_2$O$_4$ Cathode Material upon Charge/Discharge. *Chem. Mater.* **2014**, *26*, 3535−3543.

(27) Wu, Q.; Liu, Y.; Johnson, C. S.; Li, Y.; Dees, D. W.; Lu, W. Insight into the Structural Evolution of a High-Voltage Spinel for Lithium-Ion Batteries. *Chem. Mater.* **2014**, *26*, 4750−4756.

(28) Feng, X.; Yang, Z.; Tang, D.; Kong, Q.; Gu, L.; Wang, Z.; Chen, L. Performance Improvement of Li-Rich Layer-Structured Li$_{1.2}$Mn$_{0.54}$Ni$_{0.13}$Co$_{0.13}$O$_2$ by Integration with Spinel LiNi$_{0.5}$Mn$_{1.5}$O$_4$. *Phys. Chem. Chem. Phys.* **2015**, *17*, 1257−1264.

(29) Chen, Y.; Xie, K.; Zheng, C.; Ma, Z.; Chen, Z. Enhanced Li Storage Performance of LiNi$_{0.5}$Mn$_{1.5}$O$_4$-Coated 0.4Li$_2$MnO$_3$·0.6Li-Ni$_{1/3}$Co$_{1/3}$Mn$_{1/3}$O$_2$ Cathode Materials for Li-Ion Batteries. *ACS Appl. Mater. Interfaces* **2014**, *6*, 16888−16894.

(30) Long, B. R.; Croy, J. R.; Park, J. S.; Wen, J.; Miller, D. J.; Thackeray, M. M. Advances in Stabilizing 'Layered-Layered' xLi$_2$MnO$_3$·(1−x)LiMO$_2$ (M = Mn, Ni, Co) Electrodes with a Spinel Component. *J. Electrochem. Soc.* **2014**, *161*, A2160−A2167.

(31) Yu, D. Y. W.; Yanagida, K.; Nakamura, H. Surface Modification of Li-Excess Mn-Based Cathode Materials. *J. Electrochem. Soc.* **2010**, *157*, A1177−A1182.

(32) Johnson, C. S.; Li, N.; Lefief, C.; Vaughey, J. T.; Thackeray, M. M. Synthesis, Characterization and Electrochemistry of Lithium Battery Electrodes: xLi$_2$MnO$_3$·(1−x)LiMn$_{0.333}$Ni$_{0.333}$Co$_{0.333}$O$_2$ (0 < x < 0.7). *Chem. Mater.* **2008**, *20*, 6095−6106.

(33) Oh, P.; Ko, M.; Myeong, S.; Kim, Y.; Cho, J. A Novel Surface Treatment Method and New Insight into Discharge Voltage Deterioration for High-Performance 0.4Li$_2$MnO$_3$-0.6Li-Ni$_{1/3}$Co$_{1/3}$Mn$_{1/3}$O$_2$ Cathode Materials. *Adv. Energy Mater.* **2014**, DOI: 10.1002/aenm.201400631.

(34) Oh, P.; Myeong, S.; Cho, W.; Lee, M.-J.; Ko, M.; Jeong, H. Y.; Cho, J. Superior Long-Term Energy Retention and Volumetric Energy Density for Li-Rich Cathode Materials. *Nano Lett.* **2014**, *14*, 5965−5972.

(35) Zhang, J.; Wang, J.; Yang, J.; NuLi, Y. Artificial Interface Deriving from Sacrificial Tris(trimethylsilyl)phosphate Additive for Lithium Rich Cathode Materials. *Electrochim. Acta* **2014**, *117*, 99−104.

(36) Zhou, X.; Wan, L.-J.; Guo, Y.-G. Binding SnO$_2$ Nanocrystals in Nitrogen-Doped Graphene Sheets as Anode Materials for Lithium-Ion Batteries. *Adv. Mater.* **2013**, *25*, 2152−2157.

(37) Zhang, J.; Lu, Q.; Fang, J.; Wang, J.; Yang, J.; NuLi, Y. Polyimide Encapsulated Lithium-Rich Cathode Material for High Voltage Lithium-Ion Battery. *ACS Appl. Mater. Interfaces* **2014**, *6*, 17965−17973.

(38) Zheng, J.; Deng, S.; Shi, Z.; Xu, H.; Xu, H.; Deng, Y.; Zhang, Z.; Chen, G. The Effects of Persulfate Treatment on the Electrochemical Properties of Li[Li$_{0.2}$Mn$_{0.54}$Ni$_{0.13}$Co$_{0.13}$]O$_2$ Cathode Material. *J. Power Sources* **2013**, *221*, 108−113.

(39) Lin, C.-k.; Piao, Y.; Kan, Y.; Bareño, J.; Bloom, I.; Ren, Y.; Amine, K.; Chen, Z. Probing Thermally Induced Decomposition of Delithiated Li$_{1.2-x}$Ni$_{0.15}$Mn$_{0.55}$Co$_{0.1}$O$_2$ by in Situ High-Energy X-ray Diffraction. *ACS Appl. Mater. Interfaces* **2014**, *6*, 12692−12697.

(40) Han, S.; Qiu, B.; Wei, Z.; Xia, Y.; Liu, Z. Surface Structural Conversion and Electrochemical Enhancement by Heat Treatment of Chemical Pre-Delithiation Processed Lithium-Rich Layered Cathode Material. *J. Power Sources* **2014**, *268*, 683−691.

(41) Cheng, F.; Chen, J.; Zhou, H.; Manthiram, A. Structural and Electrochemical Characterization of (NH$_4$)$_2$HPO$_4$-Treated Lithium-Rich Layered Li$_{1.2}$Ni$_{0.2}$Mn$_{0.6}$O$_2$ Cathodes for Lithium-Ion Batteries. *J. Electrochem. Soc.* **2013**, *160*, A1661−A1667.

(42) Song, B.; Lai, M.; Liu, Z.; Liu, H.; Lu, L. Graphene-Involved Surface Modification on Layered Li-Rich Cathode for High-Performance Li-Ion Batteries. *J. Mater. Chem. A* **2013**, *1*, 9954−9965.